Nuclear Technology

ISSN: 0029-5450 (Print) 1943-7471 (Online) Journal homepage: https://www.tandfonline.com/loi/unct20

Visualization of Mass Transfer Between Source and Seeping Water in a Variable Aperture Fracture–Impact of Tracer Density

Helen Winberg-Wang & Ivars Neretnieks

To cite this article: Helen Winberg-Wang & Ivars Neretnieks (2020): Visualization of Mass Transfer Between Source and Seeping Water in a Variable Aperture Fracture–Impact of Tracer Density, Nuclear Technology, DOI: 10.1080/00295450.2020.1712951

To link to this article: https://doi.org/10.1080/00295450.2020.1712951

Published online: 21 Mar 2020.

NUCLEAR TECHNOLOGY

DOI: https://doi.org/10.1080/00295450.2020.1712951

Visualization of Mass Transfer Between Source and Seeping Water in a Variable Aperture Fracture–Impact of Tracer Density

Helen Winberg-Wang* and Ivars Neretnieks

Royal Institute of Technology, Department of Chemical Engineering, Stockholm, Sweden

Received November 14, 2019
Accepted for Publication January 3, 2020

Abstract — *An experiment with a vertical slot with horizontally seeping water with a dye diffusing from below was performed to help validate and visualize the Q-equivalent model, which describes the mass transfer rate from a source into flowing water, such as that in a repository for nuclear waste. The Q-equivalent model is used for quantifying mass transport in geological repositories. However, the tracer propagated much slower and to a lesser extent than predicted by the model. It was found that the tracer gave rise to a small density gradient that induced buoyancy-driven flow, overwhelming that driven by the horizontal hydraulic gradient. This dramatically changed the mass transfer from the dye source into the water in the slot. For the release of contaminants, this can have detrimental as well as beneficial effects, depending on whether positive or negative buoyancy is induced. These observations led to an analysis of when and how density differences in a repository can influence the release and further fate of escaping radionuclides in waste repositories. This and other experiments also showed that laboratory experiments aimed at visualizing flow and mass transfer processes in fractures could be very sensitive to the heating of the dye tracers by the lighting in the laboratory.*

Keywords — *Tracer experiments, repositories, safety assessment.*

Note — *Some figures may be in color only in the electronic version.*

I. INTRODUCTION

The Swedish method of disposal of high-level nuclear waste, called KBS-3, utilizes three barriers. The waste is encapsulated in copper canisters and placed in holes in the bedrock at a depth of about 500 m. The canisters are embedded in compacted bentonite clay. The third barrier is the rock itself. The equivalent flow rate $Q_{eq,}$ quantitatively describes the transport capacity of solutes, including radionuclides, to seeping groundwater in the rock. It is used to quantify the release rate of radionuclides from a leaking copper canister. It can also be used to assess the rate of transfer of corrosive agents from the groundwater to the canister.

SKB is the organization responsible for designing and building the Swedish repository. SKB must demonstrate that there is a negligible risk that humans will ever be exposed to dangerous levels of radiation. This implies in practice that the function of the important components in the repository must be ensured for hundreds of thousands of years. It is not possible to design and perform human-made tests that can demonstrate this. Instead, one has to rely on the fundamental laws of physics and chemistry, such as thermodynamics, when building quantitative prediction models of all the processes involved. The possible long-term corrosion of the copper canister, for example, relies on the fact that copper does not corrode in anoxic water unless corrosive agents such as oxygen or sulfide are transported to the canister in sufficient amounts. The same transport capacity is important to assess the release rate of radionuclides from any potentially breached canister. The transport

*E-mail: helenwi@kth.se

capacity of the water seeping into the fractured rock mass is, therefore, a key issue. The transport capacity of solutes is the main theme of this paper.

One key question is how to assess the solute transport between water seeping into the fractures in the rock and the canister embedded in the protective bentonite clay. For the KBS-3 repository, the transport capacity of the seeping water is modeled as a diffusion process between the bentonite clay and the water seeping past in the fractures. This can be summarized in an entity called the equivalent flow rate denoted by Q_{eq}, as described by Neretnieks.[1]

Because the equivalent flow rate plays a significant role in the modeling of transport processes, there is a desire to experimentally visualize and validate the process and to assess the uncertainties involved in its use. This paper describes an experiment that was designed to this end. It also describes some of the difficulties encountered that influence the assessment of the magnitude of the Q-equivalent. Some of the difficulties encountered, such as buoyancy-induced flow and instabilities in tracer systems, have already been elaborated and are presented in Refs. 2, 3, and 4.

In the case of a leaking copper canister, released water-soluble radionuclides can diffuse out into and through the surrounding compacted clay. The nuclides then diffuse from the clay into water seeping into rock fractures intersecting the deposition hole. This experimental study focuses on the clay-boundary interface, where contaminants diffuse from the clay-water interface to the seeping water in the rock fractures. The rate-limiting step has been found to be the diffusion from the clay-water interface into the water. The approaching water has a concentration c_w. For radionuclides, it is in practice zero, but for intruding corrosive agents it is a value larger than that at the corroding copper surface. For long diffusion times, the solute flow rate N will reach steady state and can be described by the equivalent flow rate times the driving force, which is the concentration difference between the clay-water interface c_o and the concentration of the approaching water c_w:

$$N = Q_{eq}(c_o - c_w)\,. \tag{1}$$

The equivalent flow rate depends on fracture aperture b, length of clay-water interface l, diffusion coefficient in water D_w, and water residence time t_w of the water as it passes the clay-water interface. The N expression for the Q-equivalent was derived by solving the diffusion equation for the uptake into the seeping water.[1] Different applications and examples of its use can be found in Ref. 5, where other resistances to the release rate also are elaborated, including the diffusion resistance in the clay. The Q-equivalent concept is convenient to use in performance assessment simulations because of its simplicity and because it is essentially independent of the type of solute. This is because small molecules and ions have very similar diffusion coefficients. For a plane interface, the expression is

$$Q_{eq} = 1.13b\sqrt{D_w l u} = 1.13bl\sqrt{D_w/t_w}\,. \tag{2}$$

There is a desire to experimentally demonstrate and validate the simple formula. In an earlier paper (Ref. 2) this was done experimentally in one way. In this paper another different experiment is described.

The basic model assumes a parallel plate fracture, constant or slowly changing source concentration, and laminar flow. Previous work by Liu and Neretnieks[6,7] showed by stochastic simulations that the simple Q-equivalent model works well also for diffusion and flow in variable fractures and at various intersection angles between fracture and the deposition hole.

This paper describes the design of the experimental equipment and the experiment and modeling used to evaluate the experiment. The work aims to bridge the gap between model and reality by experimental validation at times long enough for the system to reach steady state in variable aperture fractures. It addresses the severe effects of even small density gradients caused by the diffusing dye used for visualization. The density changes caused by the dye considerably influence the tracer experiments by generating buoyancy-driven flow.

II. EXPERIMENTS

The experimental setup was constructed by the assembly of two sheets of wavy glass. The setup is intended to simulate a variable aperture rock fracture. The fracture was attached to a dye source at the bottom to represent a radionuclide. The fracture was set, and vertical and horizontal water flow was pumped through it.

II.A. Experimental Setup

The fracture was made of two pieces (150 × 150 mm) of shower cabin glass in contact (1) (see numbers in Fig. 1) to provide the variable aperture. The fracture was kept in place by a frame of acrylic glass. The fracture was connected to a buffer chamber (2) filled with glass wool to prevent convection in the source chamber. Table I gives the dimensions. Below the buffer chamber, a filter paper (3) was inserted to keep the dye in place while filling the dye chamber (4). On each side of the fracture, there is a vertical pressure distribution chamber (PDC)

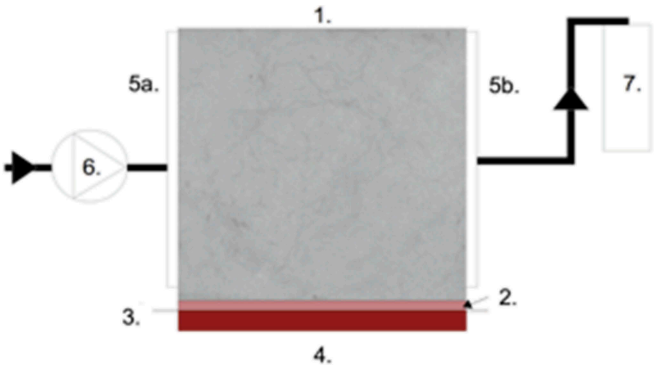

Fig. 1. Experimental setup with seeping water: (1) artificial fracture, (2) buffer chamber, (3) filter, (4) dye chamber, (5a) PDC on left side, (5b) PDC on right side and sealed at the upper edge, (6) pump, and (7) effluent collection.

(5a and 5b), starting 16 mm above the buffer chamber, which was also filled with glass wool. The PDCs were intended to ensure that the hydraulic head along the vertical slot between the two glass sheets is essentially constant along the inlet as well as along the outlet. The water was pumped (6) into the left PDC via a tube, and the effluent was collected from a vial (7) connected to a tube going from the outlet PDC. To seal the setup, silicon glue was applied and allowed to harden before the run. Next to the main fracture, a tapered calibration slot was in place (see Sec. II.A.1). The inlet and outlet were located at mid height of the glass sheets, which was around 7 cm above the bottom of the fracture.

To measure the aperture in the fracture, light absorption of the dye was measured, and Lambert-Beer's law was used to derive aperture from measured light absorption (see Sec. II.C). A light board was placed behind the setup to provide even background lighting, and a camera (Nikon D90) was placed in front of the setup to photograph the light transmitted through the setup. The camera was connected to a computer for taking a time-lapse photo each day (Camera Control Pro 2, commercially available software from Nikon).

II.A.1. Aperture Measurement

A vertical tapered calibration slot was used to measure the aperture in the fracture. The slot was constructed of two plane-side-fazed glass plates 150 mm long and 3 mm thick. The slot was made by joining the glass at the bottom and letting spacers, small pieces of plastic, separate the glass at the top to create a wedge. The wedge aperture ranged from 0 mm at 3.5 mm from the bottom to about 1.3 mm at the top. The bottom and sides were sealed with silicon. The outside was equipped with a ruler starting from the bottom.

For the aperture measurement, the slot was filled with a diluted dye with a fraction 1/10 of the dye chamber concentration. The variable aperture fracture was filled with the same dye solution; thereby, the aperture in the fracture could be determined. This was done by matching the intensity in each point of the fracture with the intensities obtained in the calibration slot after it was adjusted for minor unevenness in the background lighting. The details of the image processing can be found in Sec. II.C. This was done by photographing the light board and locating the fixed points used to identify the location of the light board. The resolution of the camera was set to give about 3 to 4 million pixels, which gives a resolution of less than 0.1 mm.

II.A.2. Dye

The dye chosen for the experiment was a commercial carminic acid solution (CA) (Dr. Oetker). Carminic acid was chosen because of its relatively low degradation over time (estimated from the photographs to about 10% after 96 days) and relatively small molecule size. Furthermore, the CA did not react significantly with the frame material and possesses high color intensity even at low concentrations. The density of the undiluted CA was measured with a 100-mL pycnometer. Its density is 1.0% larger than that of pure deionized water at room temperature.

TABLE I

Experimental Setup Dimensions

	Height (mm)	Depth (mm)	Length (mm)	Volume (mL)
Fracture	150	~0.36	150	~8[a]
Dye chamber	11	15	148	30
Buffer chamber	9	3.5	148	5
PDC	125	3	3.5	2

[a]Determined by the experiment.

With the molar volume 263.4 cm^3/mol (Ref. 8), the diffusion coefficient of the CA was estimated with the Siddiqi-Lucas correlation[9] to be $4 \cdot 10^{-10}$ m^2/s at 20°C.

The flow experiment was taken to have reached the steady state when the effluent concentration had leveled off. The effluent concentration was determined by measuring the light absorption, at the peak $\lambda = 512$ nm, with a spectrophotometer (Hitachi U-2100). The extinction coefficient was determined by measuring the absorption of a series of diluted CAs to obtain any deviations from Lambert-Beers law.

II.A.3. Filter

The filter paper was a 120H hard filter from Munktell. The filter resistance was determined by separate experiment with another tracer. It was found to be $1/1.38 \times 10^{-7}$ m/s for fluorescein. Fluorescein is a slightly smaller molecule than the CA. Because of their relatively close molecule sizes, the filter resistance was assumed to be valid for both dyes. The filter resistance becomes negligible already after a few days of the experiment.

II.A.4. Pump

The pump was a programmable HPLH-pump from CAT, type VS. To obtain the desired low flow rate of 55 μL/h, a periodic flow was used. The flow rate, 0.1 μL/s, was maintained for 4.5 min, followed by a 25-min delay. This gave a water residence time of 5.1 days in the slot. This was estimated to be long enough for the 1% tip of the diffusion profile to reach 5 cm before arriving at the outflow end.

II.B. Experiment

The experiment was prepared by filling the setup with degassed deionized water. This was done by letting the pump slowly pump water into the setup and removing the air from the top right corner by a valve. After the setup was filled and trapped bubbles reduced, the dye solution was introduced into the dye chamber. The dye chamber was filled by connecting one of the valves to a vial with concentrated dye. The vial was placed at a higher level. Thereafter a syringe was used to initiate the flow of dye from the other side of the dye chamber by removing a small volume of water (10 ml at the time). After about five dye chamber volumes had passed, the valves were closed. At that time the pump was turned on, the valve for the effluent opened, and a photograph was taken once every 24 h for a few months.

II.C. Image Processing

To determine the fracture aperture, the photographic images were processed with Matlab®. Lambert-Beer's law was applied. Lambert-Beer's law describes the intensity of the transmitted light I_s as a function of a dye dependent on its extinction coefficient ϵ, aperture b, and the solute concentration c:

$$\frac{I_s}{I_0} = 10^{-\epsilon c b}, \tag{3}$$

where I_0 is the intensity of the background lighting. Sawada[10] and Isakov[11] used a similar technique to study the flow and solute transport in variable aperture fractures.

Equation (3) was applied as follows. First, the photos were intensity calibrated by dividing the intensity $I_s(x,y)$ of each pixel with the background intensity of the light board in that pixel $I_0(x,y)$ to account for any setup shadows and backlight unevenness. The change in background light intensity with time was slight but was corrected for by comparison with that in the dye-free zones.

Second, the aperture was determined by utilizing the light intensity in the calibration slot. The known aperture and concentration in the calibration slot were used to determine the light extinction coefficient ϵ as a function of $\frac{I_s}{I_0}$. There was only a slight deviation from Lambert-Beer's law. By using this correction, the aperture in the fractures was determined. However, the measurement gave slightly negative values for the narrowest zones. This was compensated for by increasing the entire aperture by 0.05 mm so even the narrowest points became positive or zero. The number of aperture data points of the fracture was reduced to a 121×121 matrix, 1 mm^2/cell to save computational effort in the subsequent simulations. The smaller concentration fine structure that was lost by lumping the pixels into 1×1 mm^2 would be evened out by diffusion during a time of about 1 h.

To be able to account for the areas that were not available to the camera (about 1 cm shaded by silicone and frame), a cokriging function[12] was applied. A kriging function is used for spatial estimations and uses information from the spatial variation in known (visible) areas to estimate unknown areas nearby. In this case, it used the aperture variations and correlation length from the ten nearest neighbors at the border to the invisible part of the slot to numerically estimate the aperture in the hidden zone. Kriging thereby could increase the aperture matrix to 151×151, representing the entire slot.

III. EXPERIMENTAL RESULTS

The experiment ran for 105 days before being terminated due to air intrusions. This section presents the results from the aperture measurements and the effluent concentration measurement.

III.A. Aperture Field

Figure 2 shows the visual part of the slot, 120 × 120 mm^2, filled with dye during the aperture measurement. Figure 2 shows the product of concentration and aperture $c \cdot b$. As the concentration is known, the aperture distribution can be determined.

Figure 3 shows the aperture field together with areas estimated by kriging in millimeters. The mean aperture is 0.36 mm. The yellow/light green areas show the larger apertures in the fracture, which will lead to channels with higher flow, and the dark blue areas show narrow zones with less flow.

III.B. Concentration Field in Flow Experiment

Figure 4 shows an image of the dye propagation into the fracture after 96 days. This is taken to be at steady state. The flow in the setup was from left to right. The red color intensity in Fig. 4 is proportional to the product of concentration and aperture. The dye concentration in the dye chamber is ten times that used in the aperture measurement concentration (Fig. 2).

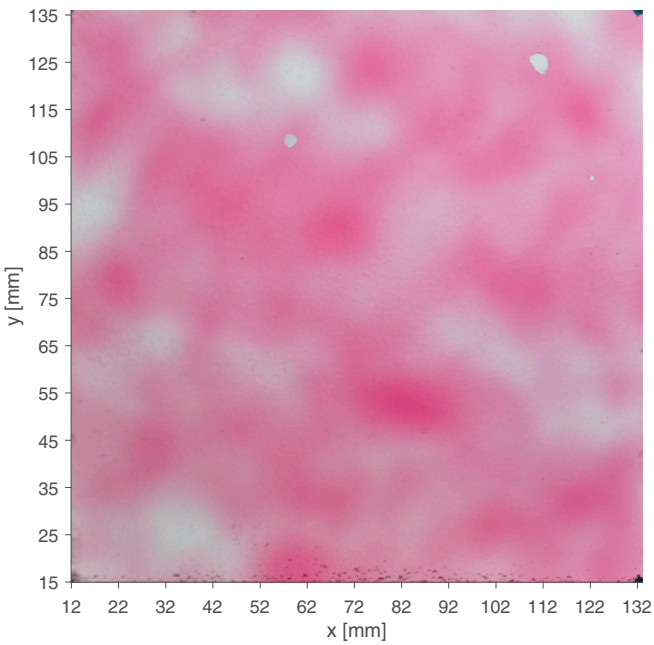

Fig. 2. Glass fracture filled with calibration solution, 0.1 × c_0.

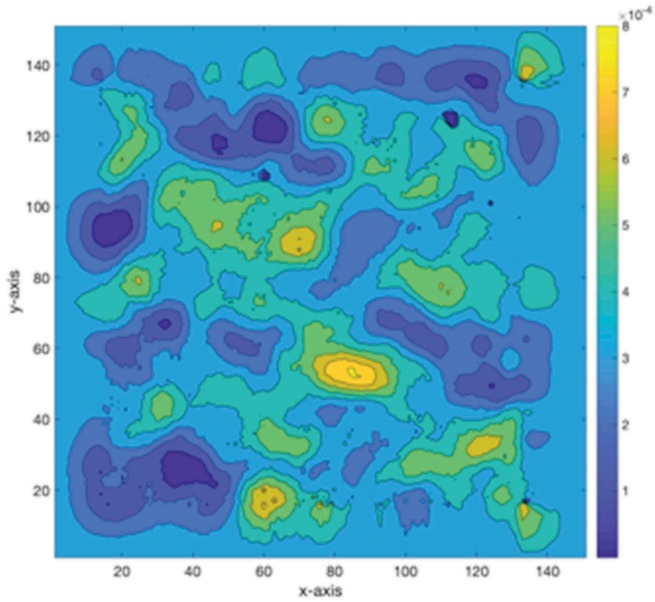

Fig. 3. Measured fracture aperture field in millimeters.

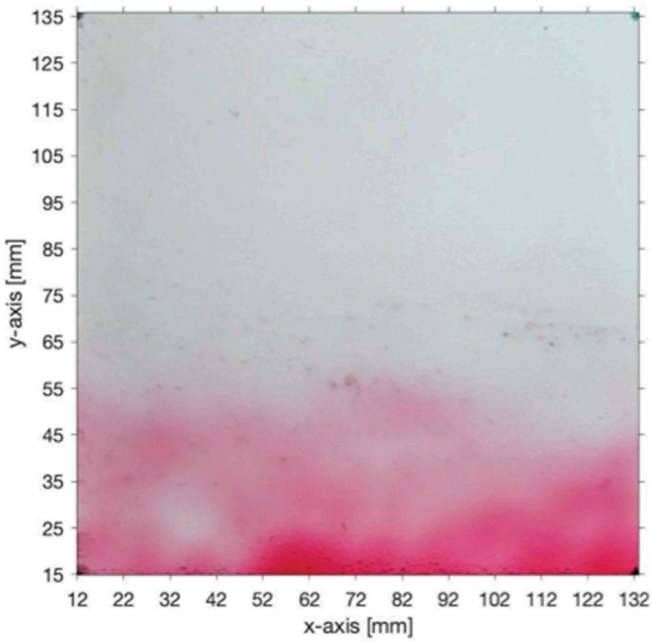

Fig. 4. Solute distribution at steady state.

III.C. Effluent Concentration

The effluent concentration was determined by measuring the light absorption of the sample vials. The dye breakthrough curve is shown in Fig. 5. The early high measurement after 15 days is due to a broken vial seal

and consequent evaporation of the sample. As can be seen in Fig. 5, the first breakthrough of the effluent concentration came after a few days, whereas it took about 80 days to get close to steady state.

The steady-state concentration is 0.003 c/c_0 and the measured equivalent flow rate is 5.6×10^{-14} m^3/s, which is about 30 times lower than what Eq. (2) gives.

IV. SIMULATIONS OF FLOW AND SOLUTE PROPAGATION

The experimental results were first compared to the simple Q-equivalent formula. Equation (2) gives an equivalent flow rate at steady state of 1.7×10^{-12} m^3/s, for a constant aperture $0.36 \times 150 \times 150$-$mm^3$ slot with the pumping flow rate used. This is a factor 30 times larger than that obtained from the experiment. The reason(s) for this large difference is sought next by some simulations in which buoyancy effects caused by the differences of water with dye and pure water were studied because considerable buoyancy-induced flow had been observed in some of our other experiments.[2]

IV.A. Using Variable Aperture Field and Neglecting Buoyancy Effects

At the time when these experiments were done, we did not anticipate that the dye density would influence the flow field and the rate of mass transfer, but assumed that the concentrations were so low that the physical properties of the water solution were the same as those of pure water. We have subsequently found that extremely low solute concentrations also can induce buoyancy forces that influence the flow field.[3,4] We therefore first show simulations neglecting buoyancy effects and then account for them to show the differences.

IV.A.1. Modeling

To simulate the experimental setup while neglecting local differences in density, a numerical model was developed. In the simulations, a two-dimensional (2-D) computational domain is considered. The simulation provides both flow field and concentration field in two dimensions.

The domain consists in the physical space of a slot with a varying aperture. We denote the coordinates along the slot by x and y, where the x-axis is along the bottom and the y-axis is height. The aperture field is denoted by $\boldsymbol{b}(x,y)$. The flow is in the positive x-direction. The flow is seeping and modeled as a laminar incompressible fluid.

The experimental aperture was determined as a discrete field. However, in order to use the experimental aperture field in COMSOL Multiphysics®, it was, with the kriging function, increased to a 161 × 161 matrix and fitted to a smooth high-order polynomial function with the

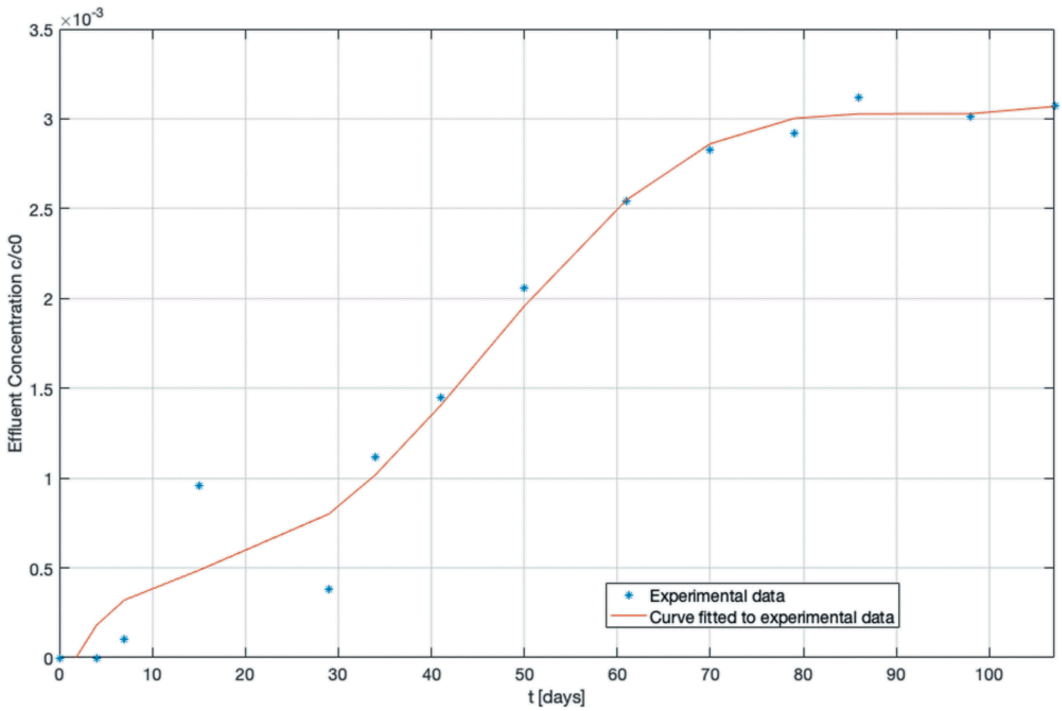

Fig. 5. Effluent concentration in the outlet as a function of time.

Polyfitn function by D'Errico.[13] Polyfitn acts in a similar manner as Polyfit but can be used for higher dimensions.

The obtained aperture field is used to determine the flow field $\mathbf{u}(x,y)$. The cubic law was used to simulate the steady-state water flow in the fracture as a function of the aperture field.[14] The cubic law states that the flow rate is proportional to the aperture to the third power for a given hydraulic gradient. The total flow rate Q through the fracture is given by the pumped flow. From this, a mean hydraulic gradient is determined by solving the Darcy flow [Eq. (4)] for the fracture:

$$\boldsymbol{Q} = -k\frac{A\rho g}{\mu}\nabla H\,, \tag{4}$$

where

A = cross-sectional area

g = gravitational constant

ρ = density

μ = viscosity of water

$k = b^2/12$ = fracture permeability.[15]

At the inlet and outlet, the hydraulic head is taken to be constant over the whole height y due to the PDCs. The lower nonflow parts of the setup, i.e., the buffer chamber and dye chamber, are disregarded in the simulations.

To model the water flow and solute transport in a variable aperture fracture, both the variable flow field and the diffusion in the variable aperture have to be coupled. In narrow rock fractures, the water flow is seeping and can be regarded as laminar and incompressible. Therefore, the flow can be described by the Darcy equation [Eq. (4)], which is a function driven by a local hydraulic head gradient. In the case of a steady-state flow, the law of conservation of mass dictates that there is no change in flow rate $\nabla \cdot Q = 0$, which is expressed by the Reynolds's equation[16]:

$$\nabla \cdot \boldsymbol{Q} = \nabla \cdot \left(-\frac{\rho g}{12\mu} b^3 \nabla H\right) = 0\,. \tag{5}$$

Solving Eq. (5) for the flow rate in the experiment and for the mean aperture, 0.36 mm, gives a mean hydraulic gradient $dH/dx = -2.6 \times 10^{-6}$ m/m. The gradient for the variable aperture fracture was found to be -3×10^{-6} m/m using COMSOL Multiphysics.[17] The numerical solution also gives the flow field.

Once the velocity field $\mathbf{u}$ has been determined, the time-dependent diffusion-convection equation is used to describe how the concentration distribution evolves with time. First, the three-dimensional diffusion-convection equation is to be reduced to a 2-D equation. In a thin fracture, it can be modeled as a 2-D fracture because diffusion across the aperture rapidly evens out any differences caused by the semiparabolic velocity profile. Therefore, the time-dependent diffusion-convection equation for a fracture with a variable aperture can be written as

$$\frac{\partial c_A}{\partial t} = -\boldsymbol{u}\cdot\nabla c_A + D_w\nabla^2 c_A + \frac{D_w \nabla \mathrm{b}\cdot\nabla \mathrm{c}_A}{b}\,, \tag{6}$$

where the last term accounts for the local variations in the aperture in the fracture.

Initially, the fracture is filled with pure water, $c = 0$, and all dye is confined to the dye chamber, the bottom border of the simulation domain. The dye diffuses into the water-filled fracture from the solute source boundary where the concentration is c_o. The upper boundary is closed to diffusion. The inflowing water has a concentration of $c = 0$. The concentration at the outflow boundary is found from the solution of Eq. (6).

IV.A.2. Results

The flow field is illustrated in Fig. 6. The flow paths are illustrated by the streamlines. Figure 7 shows the simulation results of the diffusion-convection equation after steady state has been reached.

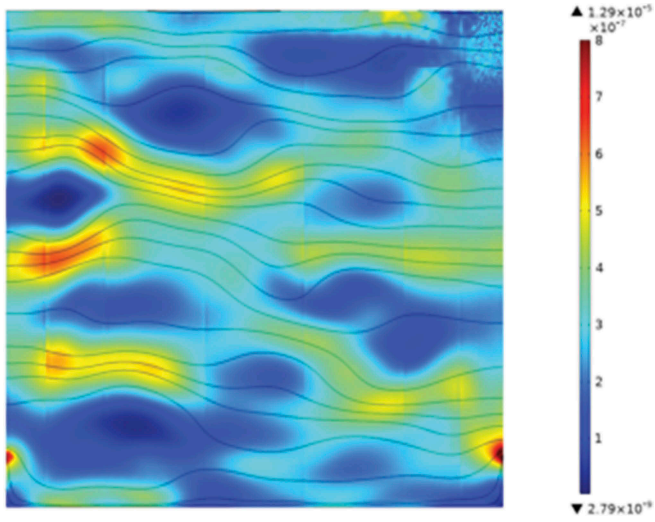

Fig. 6. Velocity magnitude in meters/second (and magnitude-controlled streamlines determined by the cubic law).

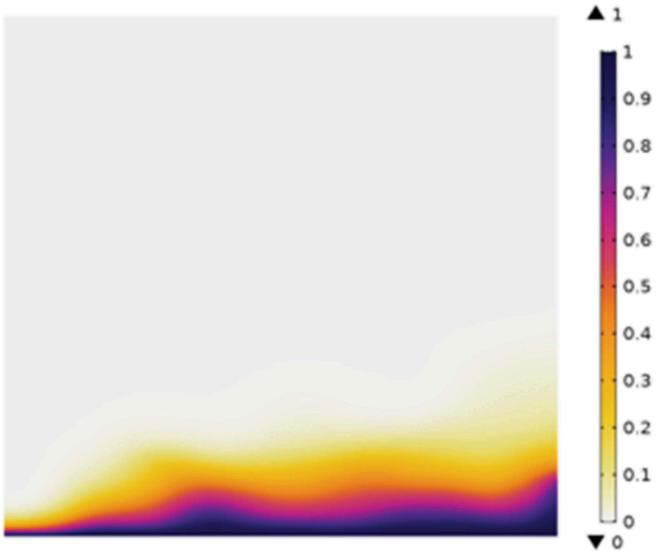

Fig. 7. Solute concentration (color bar shows c/c_o) in the fracture at steady state.

When comparing the experimental dye propagation with the simulation concentration profile, it can be seen that the shape is very different. Compared with Fig. 4, the experimental profile is essentially even along the x-axis, whereas the simulation shows an increase of carmine penetration the longer the water is in contact with the dye chamber. The simulation also gives shallower penetration than the experiment. The effluent concentration in the simulation was practically zero.

Another simulation was made to compare the effect of the aperture variation. It was run with a constant aperture $b_p = <\boldsymbol{b}(x,y)>$. The difference in the equivalent flow rate Q_{eq} is shown in Fig. 8. It shows that it is fair for the purpose of solute transport modeling to approximate the variable aperture with its mean value in this case. It is seen that after a little more than 5 days (one residence time) as expected, the effluent concentration has reached steady state. This is in contrast to about 80 days in the experiment.

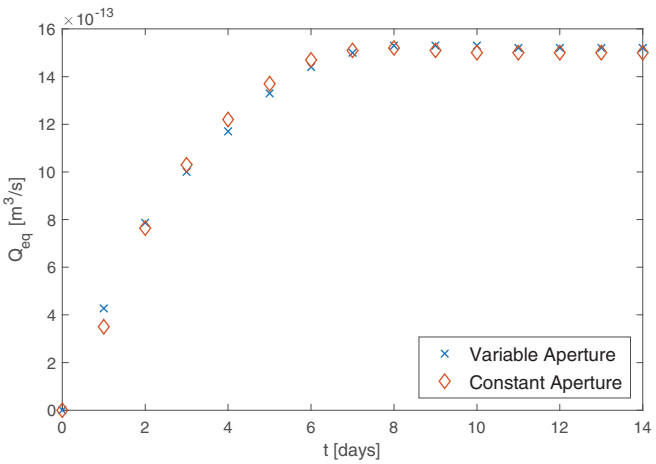

Fig. 8. Q_{eq}, as a function of time for variable aperture slot compared to constant aperture slot.

Furthermore, the large differences in the effluent concentration and Q_{eq} at steady state between the experimental result ($Q_{eq} = 5.6 \times 10^{-14}$, $c/c_o = 0.003$) compared to the simple formula ($Q_{eq} = 1.7 \times 10^{-12}$ m^3/s) and the simulation ($Q_{eq} = 1.5 \times 10^{-12}$ m^3/s, $c/c_o = 0.1$) led to considerable work to search for the reasons for the discrepancies. It included testing other tracers, such as uranine instead of carmine, which led to other problems that are explored in Ref. 4. Some tests suggested that the negative buoyancy of the slightly denser carmine solution changed the flow path of the water substantially, hindering it from moving the dye up to the outlet point located halfway up the fracture.

IV.B. Impact of Dye Density Effects

Scoping calculations showed that even a very slightly denser dye solution would prevent the dye from being brought up to the outlet location. It would have to diffuse upward toward the exit level to flow out from the chamber. This effect can be illustrated by a comparison of the mean hydraulic gradient induced by pumping, which is equivalent to 2.6×10^{-6} m/m, and the density difference between the dye solution and the adjacent water without dye. The buoyancy-induced gradient $\frac{\Delta\rho}{\rho}$ is about 0.01 for the carmine solution to water. This can generate a buoyancy-driven gradient more than 1000 times larger than the hydraulic gradient. It will still be significantly larger even when it has been diluted several hundred-fold.

This implies that the hydraulic gradient, even if it were directed upward, cannot lift the water up from the bottom of the fracture where the dye enters to the level of the outlet location about 7.5 cm higher up. The carmine will accumulate in the lower part of the fracture and in both PDCs. In the inlet PDC the carmine will enter by backflow as well as by diffusion. There will be negligible flow in the region below the level of the inlet and outlet locations at 7.5 cm above the top of the buffer chamber. Above this level, the water will flow nearly horizontally to the outlet, carrying with it the dye that enters the seeping water from below by diffusion. At early times when the dye has not yet reached the effluent height, no or very little dye is found in the effluent. Gradually the concentration will build up and reach a steady state.

IV.B.1. Analytical Approximation

To further illustrate and in a simple way model this case, we derive a simple approximate model. The inlet and outlet are located just above mid height of the glass sheets. When the dye that diffuses up from the dye chamber makes the water with dye denser than pure water, it must be lifted up to the effluent level at mid height of the fracture before it can flow out. The hydraulic gradient must overcome the negative buoyancy of the dyed water. The relative density difference is $(\rho_{dyed} - \rho_w)/\rho_w$, which must be smaller than the vertical pressure gradient dH/dy to lift the dyed water to the effluent location. In Sec. IV.B.3, detailed numerical simulations are presented. In this section, we explore the consequences of the case when the dyed water cannot be lifted by using a simplified analytical approach described below

When the water close to the source diffuses into the water above it, it cannot be lifted and there is no flow in the lower part of the fracture. Water flows only where the relative density difference is less than the hydraulic gradient. Eventually, the dye diffuses up to the level of the effluent. At this level, the water with dye need not be lifted and can flow out. This is the basis for the following idealized model concept.

In the beginning, when the slot is filled with pure water dye diffuses upward and eventually reaches the level of the outlet and can start to flow out. At the interface between the flowing water above and the stagnant water below, the solute concentration becomes constant and is equal to c_{int}. From the interface, solute diffuses up into the seeping water above and is carried toward the outlet by the flow. Once underway it is fed by more and more solute diffusing into the seeping water. The process is fully analogous to the Q-equivalent concept in which there is a clay-water interface.

This somewhat idealized process can be modeled analytically as follows. Consider the steady-state situation where the concentration in the region between the bottom of the fracture, $y = 0$, is c_o, and the concentration at outlet level, $y = y_{outlet}$, i.e., at the interface between stagnant and the flowing water, is c_{int}. At this level, the mass flux at the interface is equal to the outflow concentration times the total volumetric flow rate:

$$N = c_{int} \times Q_{eq(int)} = c_{outlet} \times Q_{tot} \,, \tag{7}$$

where c_{outlet} is the concentration in the flow rate through the equipment Q_{tot}.

At steady state, the concentration gradient below the interface is constant and equal to $\frac{c_o - c_{int}}{y_{outlet}}$. Therefore, the inflow rate from the dye chamber can be expressed as

$$N = A * \frac{c_o - c_{int}}{y_{outlet}} * D_w \,, \tag{8}$$

where A is the cross-section area of the fracture $b_{mean}x_o$, and Q_{eq} is obtained through the simple formula [Eq. (2)] as a function of the pump flow rate Q using the water residence time in the fracture above y_{outlet}.

Setting Eq. (7) equal to Eq. (8), sets $c_o = 1$, and solving for c_{int} gives

$$c_{int} = \frac{c_o}{1 + \frac{Q_{eq(int)} y_o}{D_w x_o b}} \,. \tag{9}$$

For the experimental conditions, this gives an outflow concentration $c_{int} = 0.108\ c_o$.

The concentration evolution over time in the slot can be obtained for the model from the diffusion equation:

$$\frac{\partial c}{\partial t} = D_w \frac{\partial^2 c}{\partial y^2} \,, \tag{10}$$

with the initial condition and boundary conditions of $c = 0$ at $t = 0$, all y, and $c = c_o$ at $y = 0$, $t > 0$:

$$D_w b x_o \left.\frac{\partial c}{\partial y}\right|_{y=y_{outlet}} = -Q_{eq(int)} \,. \tag{11}$$

As Fig. 9 shows, the simulated effluent concentration builds up with time, indicating a steady state established first on the order of 100 days.

Equation (7) gives $c_{outlet} = 0.0168\ c_o$. This is still 5.6 times larger than the measured value.

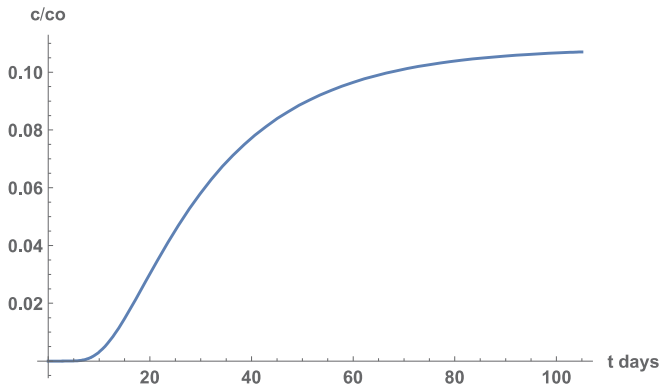

Fig. 9. Effluent concentration evolution over time.

IV.B.2. Numerical Simulations Accounting for Buoyancy Effects

The simple model above assumes that there is a sharp boundary at the effluent height above which all water with dye is swept away. This is an approximation and a more accurate simulation is now used in which more details of the experimental setup are used. The wide vertical PDCs on each side of the fracture are accounted for. The concentration impact on the buoyancy in every point is accounted for. Very minor concentration differences are expected to strongly impact the magnitude and direction of the hydraulic head gradient. It is therefore explored if this, together with the presence of the highly conductive pressure chambers, can explain the experimental results.

To simulate the system, including the effect of density on the system, the PDCs have to be included. As before the system is reduced to a 2-D domain with a constant aperture. To account for the density dependence, the density-dependent steady-state flow field and the steady-state diffusion-convection equation are to be solved simultaneously. This makes the equations nonlinear, which complicates the solution.[18] Darcy's law describes the flow field, where the density is concentration dependent. The system of equations to solve are given below:

$$\mathbf{0} = \nabla \cdot (\rho(c)\boldsymbol{u}) \tag{12}$$

and

$$\boldsymbol{u} = -\frac{k_{bouy}}{\mu}(\nabla p + \rho(c)g) \ . \tag{13}$$

The pressure is initially $p = \rho_o g h$ as there is only pure water in the fracture. The density later becomes a function of the bulk water initial density plus the increase in density due to the dye. At low concentrations, it can be approximated to be linear:

$$\rho(c) = \rho_o\left(1 + \beta \cdot \frac{c}{c_o}\right) \ . \tag{14}$$

The effect of the PDCs is given by Eqs. (15) and (16):

$$k_{bouy} = \frac{{b_{bouy}}^2}{12} \tag{15}$$

and

$$b_{bouy} = \begin{cases} b_{\mathrm{PDC}} & x \geq 0.15\ m \\ b_p & 0.15 > x \geq 0\ m \\ b_{\mathrm{PDC}} & x < 0\ m \end{cases} , \tag{16}$$

where b_{PDC} is the aperture of the PDC. The concentration profile at the inlet is defined by the steady-state diffusion-convection equation [Eq. (17)]. The inflow from the left is defined as a Danckwerts boundary condition with a concentration in the incoming water $c = 0$. The Danckwerts boundary condition allows a discontinuity of the concentration to the left and the right of the inlet boundary (terms on the right side):

$$0 = u \cdot \nabla c - D_w \nabla^2 c \ . \tag{17}$$

IV.B.3. Results

The aperture is approximated to be constant. This simplifies the numeric computations and is reasonable considering the minor differences found earlier, as shown in Fig. 8.

Figure 10 shows the predicted flow field and the concentration distribution at steady state in the case of no density difference, $\Delta\rho = 0$ kg/m^3. The outflow concentration was $c/c_o = 0.094$ and the equivalent flow rate $Q_{eq} = 1.4 \times 10^{-12}$ m^3/s. This agrees with the simulation in the variable aperture neglecting buoyancy.

Figure 11 shows streamlines, flow vectors, and concentrations for $\Delta\rho = 10$ kg/m^3. The concentration profile along the flow direction is practically constant. The horizontal flow below the effluent location is practically zero

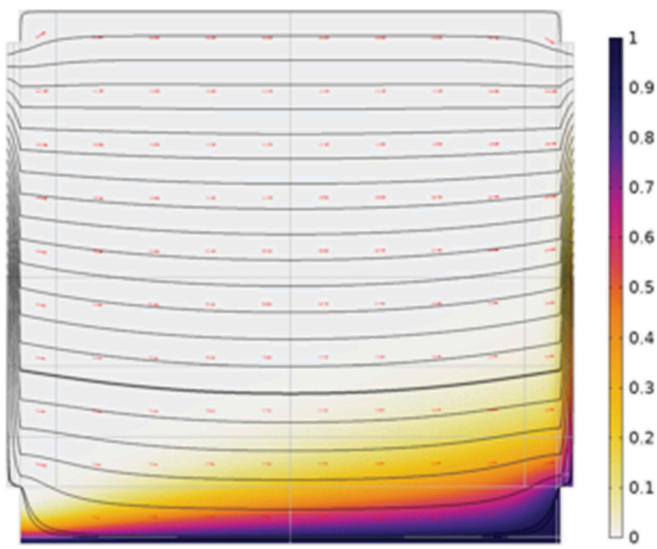

Fig. 10. Concentration distribution at steady state for $\Delta\rho = 0$ kg/m^3.

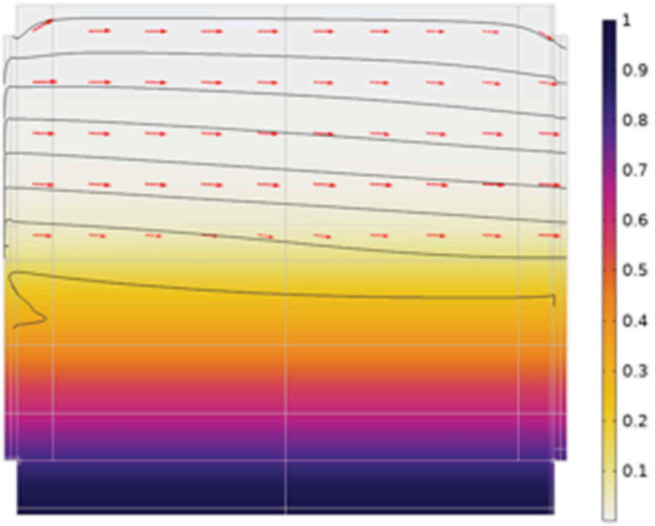

Fig. 11. Concentration distribution at steady state for $\Delta\rho = 10$ kg/m^3.

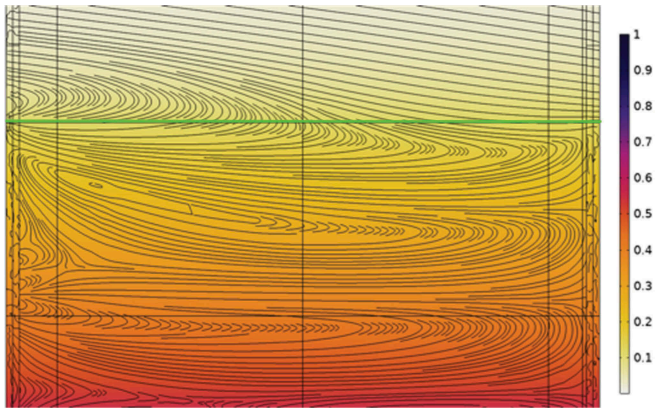

Fig. 12. Streamlines show circulation patterns around and below the effluent location level (illustrated by the green line).

because the denser liquid with the dye cannot be lifted. All the water flow is practically only above the effluent location, indicated by the horizontal weak blue line at mid height.

Table II describes how the effluent concentration and the equivalent flow rate at steady state change with the density difference between the water and dye solution. It also shows the mass flux from the bottom (y-direction) compared to the mass flux (x-direction) in the middle of the effluent PDC. The agreement of the mass balance is good.

Already a small relative density difference 10^{-4} (0.1 kg/m^3) decreases Q_{eq} by a factor of nearly 5. The simulated outflow concentration is 5.7 times larger than the experimental value and is in good agreement with what the simple analytical model gives.

The water flow below the effluent location is not entirely stagnant, however. There is very slow flow in the backward direction, and complex circulation patterns develop below this level. This is shown in Fig. 12. The effluent location is indicated by the green horizontal line, about a quarter from above. The back circulation develops because when the dye diffuses upward into the water stream flowing to the right, there is the tendency to develop a concentration profile such as depicted in Fig. 10. Because the fluid at a given height would tend to be denser in the x-direction the buoyancy difference will force the concentration to even out by inducing flow toward the left as shown in Fig. 12. Such complex circulation patterns are well known to develop in density-driven flow.[19]

V. DISCUSSION AND CONCLUSIONS

By comparing the dye distribution in the experiment after 96 days (see Fig. 4) with the ones obtained from the simulations with different density gradients (Figs. 10 and 11), it can be seen that the experiment agrees better with the one with a significant density difference. Further, from Table II one can see a clear overlap between the results from the simple Q-equivalent formula and the simulation for

TABLE II

Simulated Effluent Concentration c/c_o and Outflow as a Function of the Density Difference Between the Dye Solution and the Bulk Water at Steady State

$\Delta\rho$ (kg/m^3)	c/c_o in Effluent	Q_{eq} (m^3/s) from Effluent Concentration Times Flow Rate	Q_{eq} (m^3/s) from In-Diffusion from Bottom $y = 0$
0	0.094	1.4×10^{-12}	1.3×10^{-12}
0.1	0.02	3.2×10^{-13}	3.2×10^{-13}
1	0.018	2.7×10^{-13}	2.6×10^{-13}
10	0.017	2.6×10^{-13}	2.6×10^{-13}

a density difference of 0 kg/m^3. Table II also shows that the equivalent flow rate is very similar for density differences above 0.1 kg/m^3, and a further increase in density difference is not expected to change the equivalent flow rate much more. Both the analytical solution and the numeric simulations predict an equivalent flow rate about a factor 5 higher than the one found by the experiment. The reason for this deviation is not apparent. It may be partly due to the impact of the aperture variations. In the simulations of flow and transport in stochastic variable aperture fractures performed by Liu and Neretnieks[6,7] considerable variations in Q-equivalent values were found between different realizations. The aperture distribution nearest to the source had a huge impact. An important conclusion of this study is that in even quite narrow fractures, small density differences can give buoyancy effects that alter the flow pattern and affect the mass transfer rate.

For the release of waste to the biosphere, the experiments suggest that the release rate to the seeping water is less when the release is accompanied by an increase in density even if the rock is right below the repository depth. If the rock is permeable on the other hand, the higher-density contaminated plume will sink to a depth at which its density becomes equal to the groundwater density at that depth. This will further help to "isolate" the contamination because of the vertical distance it has to migrate by upward diffusion increases. The described experiments visualize and at least partly validate the impact that density differences can have beneficial as well as detrimental effects as described by Neretnieks and Winberg-Wang.[3]

Acknowledgments

We gratefully acknowledge the encouragement and financial support of SKB, the Swedish nuclear fuel and waste management company. We also thank Professor Luis Moreno for his comments and help with kriging.

ORCID

Helen Winberg-Wang http://orcid.org/0000-0002-2010-2894

References

1. I. NERETNIEKS, "Transport Mechanisms and Rate of Transport of Radionuclides in the Geosphere as Related to the Swedish KBS Concept," SM-243/108, International Atomic Energy Agency, –, p. 315 (1979).
2. H. WINBERG-WANG, "Diffusion in a Variable Aperture Slot-Impact on Radionuclide Release from a Repository for Spent Fuel," *Nucl. Technol.*, **204**, *2*, 184 (2018); https://doi.org/10.1080/00295450.2018.1469348.
3. I. NERETNIEKS and H. WINBERG-WANG, "Density-Driven Mass Transfer in Repositories for Nuclear Waste," *Nucl. Technol.* (2018); https://doi.org/10.1080/00295450.2018.1537460.
4. H. WINBERG-WANG, I. NERETNIEKS, and M. VOUTILAINEN, "A Note on the Use of Uranine Tracer to Visualize Radionuclide Migration Experiments: Some Observations and Problems," *Nucl. Technol.*, **205**, 964 (2019); https://doi.org/10.1080/00295450.2019.1573620.
5. I. NERETNIEKS, L. LIU, and L. MORENO, "Mass Transfer Between Waste Canister and Water Seeping in Rock Fractures Revisiting the *Q*-Equivalent Model," TR-10-42, SKB (2010); www.skb.se (current as of Nov. 14, 2019).
6. L. LIU and I. NERETNIEKS, "Analysis of Fluid Flow and Solute Transport in a Fracture Intersecting a Canister with Variable Aperture Fractures and Arbitrary Intersection Angles," *Nucl. Technol.*, **150**, 132 (2004); https://doi.org/10.13182/NT05-A3611.
7. L. LIU and I. NERETNIEKS, "Analysis of Fluid Flow and Solute Transport in a Single Fracture with Variable Aperture Intersecting a Canister: Comparison Between Fractal and Gaussian Fractures," *Phys. Chem. Earth.*, **31**, 634 (2006); https://doi.org/10.1016/j.pce.2006.04.012.
8. "ChemSpider"; http://www.chemspider.com/Chemical-Structure.8430568.html (current as of Mar. 26, 2019).
9. R. PERRY and D. GREEN, *Perry's Chemical Engineers Handbook, Equation (5-215)*, 7th ed., McGraw-Hill (1997).
10. A. SAWADA and H. SATO, "A Study of Hydraulic Properties in a Single Fracture with In-Plane Heterogeneity: An Evaluation Using Optical Measurements of a Transparent Replica," *Nucl. Eng. Tech.*, **42**, *1*, 9 (2010); https://doi.org/10.5516/NET.2010.42.1.009.
11. E. ISAKOV et al., "Fluid Flow Through Rough Fractures in Rocks I: High Resolution Aperture Determinations," *Earth Planet. Sci. Lett.*, **191**, 267 (2001); https://doi.org/10.1016/S0012-821X(01)00424-1.
12. D. MARCOTTE, "Cokriging Version 2.0," INRS-Oceanologie (1997); modified by C. LAFLEUR (1998).
13. J. D'ERRICO, "Polyfitn" (2006); https://se.mathworks.com/matlabcentral/fileexchange/34765-polyfitn (current as of Nov. 14, 2019).
14. P. A. WITHERSPOON et al., "Validity of Cubic Law for Fluid Flow in Deformable Rock Fracture," *Water Resour. Res.*, **16**, 1016 (1980); https://doi.org/10.1029/WR016i006p01016.
15. R. W. ZIMMERMAN and G. S. BODVARSSON, "Hydraulic Conductivity of Rock Fractures," U.S.

Department of Energy, Office of Scientific and Technical Information (1994); https://doi.org/10.2172/60784.

16. "Rock Fracture Flow," COMSOL Multiphysics®; https://www.comsol.com/model/download/383101/models.mph.rock_fracture_flow.pdf (current as of Nov. 14, 2019).
17. "Ver. 5.4, Modelling Software," COMSOL Multiphysics®; https://www.comsol.com/ (current as of Nov. 14, 2019).
18. "Buoyancy Flow with Darcy's Law—The Elder Problem," COMSOL Multiphysics®; https://www.comsol.com/model/download/554981/models.ssf.buoyancy_darcy_elder.pdf (current as of Nov. 14, 2019).
19. E. HOLZBECHER, *Modeling Density-Driven Flow in Porous Media*, 1st ed., Springer-Verlag, Heidelberg (1998).